ACS APPLIED MATERIALS & INTERFACES

Research Article

www.acsami.org

Achieving Type I, II, and III Heterojunctions Using Functionalized MXene

Youngbin Lee, Yubin Hwang, and Yong-Chae Chung*

Department of Materials Science and Engineering, Hanyang University Seoul, Seoul 133-791, Republic of Korea

Supporting Information

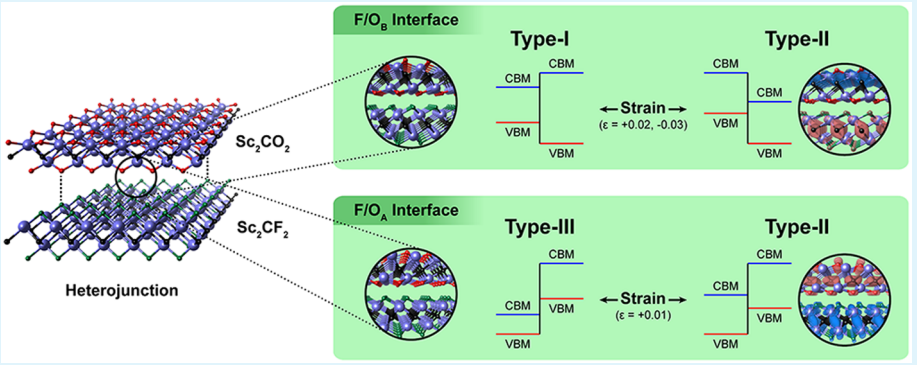

ABSTRACT: In the present work, type I, II, and III heterostructures are constructed with the same base material using three representative functionalized monolayer scandium carbides (Sc_2CF_2, $Sc_2C(OH)_2$, and Sc_2CO_2) by first-principles calculations based on density functional theory. In contrast to general bilayer heterosystems composed of two-dimensional semiconductors, type I and III heterojunctions are obtained in one Sc_2CF_2/Sc_2CO_2 system and the remains of the functionalized Sc_2C heterostructures, respectively. It is noteworthy that the same monolayer Sc_2CF_2 and Sc_2CO_2 constituents lead to dissimilar heterostructure types in the two Sc_2CF_2/Sc_2CO_2 systems by modifying the stacking interface. In addition, in the two Sc_2CF_2/Sc_2CO_2 systems, remarkable changes in the heterojunction type are induced by a strain, and two distinct type-II heterostructures are generated where one layer with the conduction band minimum state and the other layer including the valence band maximum level are different. The present work suggests an attractive direction to obtain all heterostructure types with the same base material for novel nanodevices in various fields such as photonics, electronics, and optoelectronics using only the two monolayer components Sc_2CF_2 and Sc_2CO_2.

KEYWORDS: *MXene, heterostructure, two-dimensional material, semiconductor, DFT*

INTRODUCTION

Heterostructures have been the focus of research interest to enlarge the range of available properties from single-materials.[1−14] Indeed, various heterostructures have been experimentally developed by metal−semiconductor contact or the junction of two other semiconductors.[15] They have shown attractive electronic and optical characteristics in a number of diverse fields.[5−10] In particular, the layered heterostructures fabricated by stacking different two-dimensional semiconductors like nitrides or transition metal dichalcogenides have been investigated because of their flexibility and fascinating band gap properties according to a heterojunction type.[8−15] Layered semiconducting heterostructures are considered as promising materials for the design of new devices in photonics, electronics, and optoelectronics. To fabricate a two-dimensional semiconducting heterosystem with the desired heterojunction type for the applications, many combinations of semiconductors have been widely examined.[10−13]

Recently, among these diverse two-dimensional materials, monolayer MXenes have been discovered from bulk MAX phases (M = early transition metal, A = group IIIA or IVA element, and X = carbon or nitrogen)[16−19] and have received substantial attention in various fields such as electrochemical energy storage materials and a catalyst.[19−26] MXene, which is synthesized through selective etching of the A layer in the MAX phase and sonication, consists of alternate close-packed layers of carbon or nitrogen and transition metal.[27,28] However, in a real etching process, bare MXene is spontaneously terminated by the F, OH, and O functional groups on both surfaces.[28] Although the functionalized MXenes are based on the same transition metal carbide or nitride, they have completely distinct properties according to the type of functional group.[29,30] Therefore, it is expected that a two-dimensional heterostructure with the same base material could be generated by stacking two terminated monolayer MXenes with a difference only in the functional group.

Received: January 4, 2015
Accepted: March 20, 2015
Published: March 20, 2015

DOI: 10.1021/acsami.5b00063
ACS Appl. Mater. Interfaces 2015, 7, 7163−7169

In the present work, the heterojunction type of bilayer heterostructure using three functionalized monolayer scandium carbides (Sc_2C) was studied with first-principles density functional theory (DFT) calculations. Here, three functionalized monolayer Sc_2C (Sc_2CF_2, $Sc_2C(OH)_2$, and Sc_2CO_2) were selected as the components of the heterosystem because among all the terminated MXenes, only three systems are semiconducting systems that are chemically modified by the primary functional groups that have the same base material.[28,29] Through advances in the fabrication of MXene in the foreseeable future, the terminated monolayer Sc_2C can be experimentally synthesized from bulk Sc_2AC (A = Al, Ga, In, and Tl) among the MAX phases.[31] This first exploration of the MXene bilayer heterostructure will give new insight into potential methods to effectively modulate the heterojunction type instead of the current approach of combining different materials.

CALCULATION METHOD

For the DFT calculations, the Vienna Ab-initio Simulation Package (VASP) package[32,33] was employed. All the calculations were carried out under the Perdew–Burke–Ernzerhof (PBE)[34] generalized gradient approximation (GGA) for the exchange-correlation functional with a projector augmented wave (PAW) pseudopotential method.[35] The atomic positions were optimized using the conjugate gradient algorithm until all the Hellmann–Feynman forces on each atom were less than 0.02 eV/Å. The plane wave basis was set with a cutoff energy of 520 eV, and a 12 × 12 × 1 Monkhost–Pack[36] *k*-point grid centered on the gamma point was used for the Brillouin zone integrations. The criterion for energy convergence was the 10^{-6} eV/cell, and a Methfessel–Paxton smearing scheme was used with a width of 0.1 eV. The density of states was calculated using a denser mesh of a 24 × 24 × 1 uniform *k*-point grid centered on the gamma point. Although MXene exfoliation has not been completely comprehended yet, to simulate the bilayer heterostructure of functionalized Sc_2C, all systems were modeled using a unit cell with a vacuum spacing of more than 20 Å to avoid any unnecessary interlayer reaction. The DFT-D2 method was adopted to consider the van der Waals correction for a weak interaction between the two monolayers.[37,38] Also, a dipole correction was conducted by adding an artificial dipole to the vacuum level because of the asymmetric stacking sequence.[39] To check the validity of the predicted electronic structures by the PBE functional, the band structures of three components of the heterostructures were calculated with the HSE06 functional.[40] In these cases, a 6 × 6 × 1 uniform *k*-point grid centered on the gamma point was used for effectiveness of the calculation.

RESULTS AND DISCUSSION

Before the functionalized Sc_2C heterostructure is investigated, the component monolayer systems were first studied. Each terminated Sc_2C monolayer (Sc_2CX_2, X = F, OH, and O) has four models according to the position of its functional group.[28,29] Among the models of each monolayer, one structure was selected as the constituent of the bilayer heterostructure system because it was considered as the most stable model due to its largest negative formation energy (Figure 1).[29] Unlike the Sc_2CF_2 and $Sc_2C(OH)_2$ systems, monolayer Sc_2CO_2 has an asymmetric configuration along the thickness direction because of the different sites of the O functional atoms (O_A and O_B) on both sides, as shown in Figure 1. Despite having the same components, two distinct interfaces can be induced in the bilayer heterostructure including Sc_2CO_2 due to its asymmetric structure. The unit cells of the monolayer Sc_2CF_2, $Sc_2C(OH)_2$, and Sc_2CO_2 have a lattice parameter of 3.27, 3.29, and 3.42 Å, respectively. In addition, in the calculation using the PBE

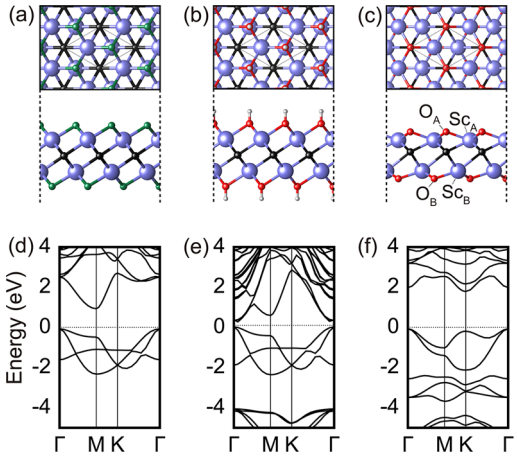

Figure 1. Most stable configuration and band structure of the functionalized monolayer Sc_2C. The top and side views of the monolayer (a) Sc_2CF_2, (b) $Sc_2C(OH)_2$, and (c) Sc_2CO_2. The purple, black, green, red, and white spheres represent the Sc, C, F, O, and H atoms, respectively. (a–c, top) The dashed rhombus indicates the unit cell. Notations of the atoms in panel c are presented due to the asymmetric structure of the monolayer Sc_2CO_2. Band structure of the monolayer (d) Sc_2CF_2, (e) $Sc_2C(OH)_2$, and (f) Sc_2CO_2. The Fermi level was set to zero.

functional, consistent with previous reports, the systems are all semiconductors,[28,29] and their band gaps are 1.00, 0.34, and 1.86 eV in Sc_2CF_2, $Sc_2C(OH)_2$, and Sc_2CO_2, respectively. Although all the systems have the valence band maximum (VBM) at the same point (Γ point), the conduction band minimum (CBM) is positioned at the *M*, Γ, and *K* points in Sc_2CF_2, $Sc_2C(OH)_2$, and Sc_2CO_2, respectively (Figure 1). The positions of the CBM and VBM and shapes of the band structures in Figure 1 correspond to the results using the HSE06 functional (Figure S1, Supporting Information). Thus, the bilayer heterostructure systems of the functionalized Sc_2C were calculated using the three monolayers with these properties in all the following computations.

When the Sc_2CX_2/Sc_2CY_2 (X/Y, X and Y = F, OH, and O) heterostructure is formed using the three monolayers mentioned above, possible high symmetry models corresponding to each interface (F/OH, O/OH (A), O/OH (B), F/O (A), and F/O (B)) were investigated (Figure S2, Supporting Information). In the O/OH and F/O heterostructures, the notations (A) and (B) indicate systems with the interface including the O_A and O_B sides of the monolayer Sc_2CO_2, respectively (Figure 1). Among the models of each heterosystem, the most stable geometries are presented in Figure 2. To confirm the stability of the most stable bilayer heterostructures, we present the strain and energies, which are generated by the heterojunction, in Table 1. Here, the strain energy (E_s) and adhesive energy (E_{ad}) of the X/Y heterostructure are defined as

$$E_s = \frac{(E_{S,X} - E_{R,X}) + (E_{S,Y} - E_{R,Y})}{A} \quad (1)$$

$$E_{ad} = \frac{(E_{S,X} + E_{S,Y}) - E_H}{A} \quad (2)$$

where $E_{S,X(Y)}$, $E_{R,X(Y)}$, and E_H represent the energy of the strained monolayer $Sc_2CX(Y)_2$, relaxed monolayer $Sc_2CX(Y)_2$, and X/Y heterostructure, respectively, and *A* is the interface

DOI: 10.1021/acsami.5b00063
ACS Appl. Mater. Interfaces 2015, 7, 7163–7169

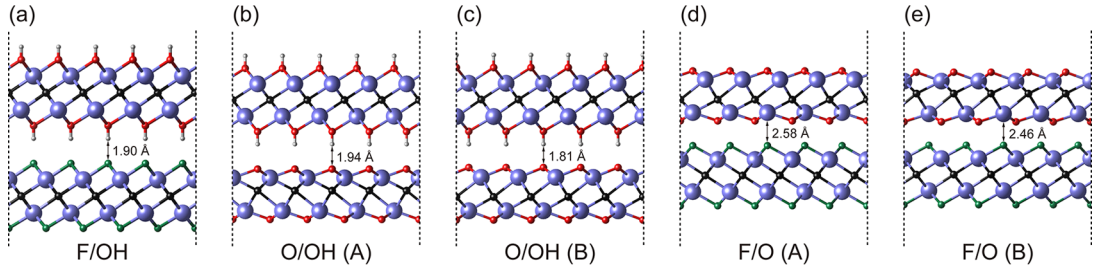

Figure 2. Most stable configuration of each functionalized Sc_2C heterostructure. The side view of the (a) F/OH, (b) O/OH (A), (c) O/OH (B), (d) F/O (A), and (e) F/O (B) heterosystems. Arrows represent the interlayer distances between the nearest atoms in the interface.

Table 1. Geometric and Energetic Properties of the Most Stable Configuration for Each X/Y Heterostructure[a]

heterostructure	a (Å)	ε (%)[b]	E_s (meV/Å^2)	E_{ad} (meV/Å^2)
F/OH	3.27	0.0/−0.6	7	36
O/OH (A)	3.36	−1.8/2.1	12	17
O/OH (B)	3.34	−2.3/1.5	23	46
F/O (A)	3.37	3.1/−1.5	17	31
F/O (B)	3.38	3.4/−1.2	18	36

[a]The listed properties are the lattice parameter of the unit cell (a), strain (ε), strain energy (E_s), and adhesive energy (E_{ad}) in the bilayer heterostructures. [b]Two values in the ε indicate the strain applied to each monolayer.

area.[8] Table 1 shows that the monolayers in the heterostructures, except for the F/OH system, are stacked in rather strained states. However, in all the functionalized Sc_2C heterostructure systems, the heterojunction lowers the total energy of the system comprised of two monolayers and leads to a more stable state by bigger E_{ad} than E_s.[8] Therefore, it is acceptable that heterostructures with such a stacking geometry could be formed.

To verify the heterojunction type of the bilayer heterostructures using the three functionalized monolayer Sc_2C, the electronic structures of these systems were studied with the band structure (Figure 3). Heterostructure composed of two semiconductors can be classified as one of three types: the type-I heterostructure (straddling gap) has the CBM and VBM states in one layer; the CBM and VBM levels of the type-II heterostructure (staggered gap) exist in different layers; and the type-III heterostructure (broken gap) has no band gap.[5,41] From Figure 3, it is clear that F/O (B) is a type-I heterostructure with the CBM and VBM states in the Sc_2CF_2 layer. Naturally, a recombination pathway of the F/O (B) heterostructure is the same as that of Sc_2CF_2 (M to Γ), and the band gap size is slightly increased to 1.21 eV compared to that of the monolayer Sc_2CF_2. On the other hand, in the other functionalized Sc_2C heterostructures, the band gaps disappear and type-III heterojunction occurs. The results are very interesting because heterostructures stacked by two-dimensional materials generally exhibit type-II heterojunction.[8,11,12,23] In particular, despite having the same monolayer components, distinct heterojunction types arise in two F/O systems. Consequently, in the bilayer heterostructures using the three functionalized monolayer Sc_2C, most of them become type-III heterostructures, but separate heterojunction types (types I and III) can be obtained using the same constituents by modulating the stacking interface in the F/O system.

Each component in the type I and III functionalized Sc_2C heterostructures is under tensile or compressive states. Also, an additional strain can be easily applied to bilayer heterosystems

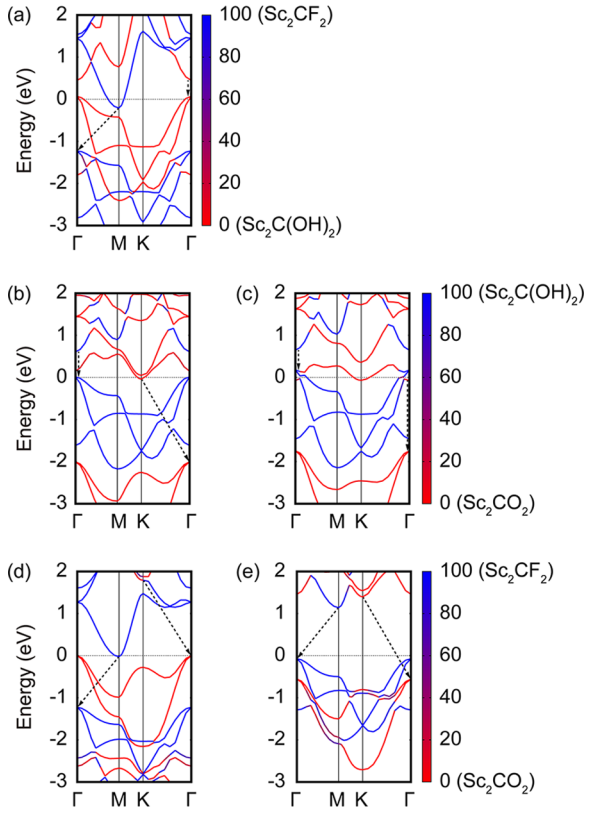

Figure 3. Band structure of each functionalized Sc_2C heterostructure: (a) F/OH, (b) O/OH (A), (c) O/OH (B), (d) F/O (A), and (e) F/O (B) systems. The Fermi level was set to zero, and the dashed arrows indicate pathways from the CBM level to the VBM level of each component in the heterostructure. The percentages of the contributions of each monolayer are marked in a different color.

by mechanical loading or a lattice mismatch on a substrate.[42] Thus, it is necessary to investigate the strain effect on the functionalized Sc_2C heterostructures because it is an important factor in determining the electronic properties of systems like other diverse low-dimensional materials.[8,42−48] When the heterostructures are influenced by the equibiaxial strain, type-III heterojunction is still preserved in the F/OH and O/OH systems (Figure S3, Supporting Information). On the other hand, it is notable that both of the F/O systems with different heterojunction types became type-II heterostructures by the biaxial strain effect (Figure 4). The F/O (A) system is changed from a type-III to a type-II heterostructure on more than about 1% tensile strain, and the type-II heterojunction is obtained from the F/O (B) type-I heterostructure by applying more than about 2% tensile or 3% compressive strain. Furthermore, another attractive result is confirmed from the calculations. In

DOI: 10.1021/acsami.5b00063
ACS Appl. Mater. Interfaces 2015, 7, 7163−7169

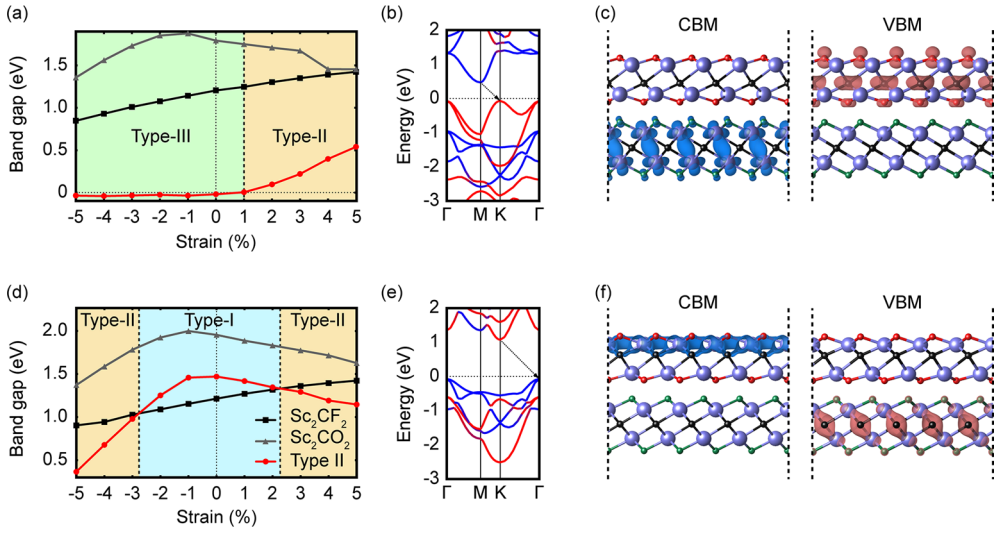

Figure 4. Electronic properties of the two F/O heterostructures under the biaxial strain. (a–c) Electronic structures of the F/O (A) and (d–f) F/O (B) systems. (a and d) Change in the energy gaps between the CBM and VBM levels of the total F/O system and each monolayer in the system as a function of the strain; energy gaps of the (black) Sc_2CF_2, (gray) Sc_2CO_2, and (red) type-II heterostructures. The energy gap of the type-II heterostructure was calculated from the difference between the CBM level of Sc_2CF_2 (Sc_2CO_2) and the VBM level of Sc_2CO_2 (Sc_2CF_2) in the F/O (A) (F/O (B)) system. The blue, orange, and green regions represent type I, II, and III heterojunction, respectively. (b and e) Band structure of the F/O system under 5% tensile strain. The Fermi level was set to zero, and the arrows indicate the recombination pathways for the excitons in each heterostructure. The percentages of the contributions of each monolayer are marked in a different color. (c and f) Charge distribution at the CBM and VBM states under 5% tensile strain. The blue and red regions represent the CBM and VBM states, respectively. The isovalue is 0.01 au.

the two strained F/O systems, the layers that include the CBM and VBM levels can be controlled by modifying the stacking interface. At the strained system with the F/O_A interface, the CBM and VBM states are located on the Sc_2CF_2 and Sc_2CO_2 layers, respectively, while the strained F/O (B) heterostructure has the CBM and VBM levels on the monolayer Sc_2CO_2 and Sc_2CF_2, respectively (Figure 4). This difference means that the CBM point and an effective mass of excitons, which are fundamentally significant for carrier transport and optical properties, can be changed by modulation of the stacking interface. Interestingly, from the results, a valuable fact is obtained that, with only two monolayers, Sc_2CF_2 and Sc_2CO_2, all the heterojunction types can be generated as type-I, two distinct type-IIs whose CBM (VBM) state exists in different layers, and type-III. The results will inspire future experiments to apply functionalized Sc_2C bilayer heterostructures to next generation solar energy conversion and electronic devices. For example, two strained F/O systems will be useful for a photocatalytic activity because the exciton recombination is reduced by a separation of the excited electron and hole.[10,41]

To clarify why such heterojunction types occur in functionalized Sc_2C bilayer systems, we first examined the bonding characteristics in the heterostructures. In general, a physical interaction is well-known as a major factor sustaining heterostructures composed of two-dimensional materials.[9,10,14,22,23] However, by comparing the binding energy ($E_b = E_{ad} - E_s$) and the interlayer distance with the previous work,[49,50] we suppose that both physical and chemical interactions between the neighboring layers are responsible for the functionalized Sc_2C bilayer heterosystems together (Supporting Information). As the chemical interaction, charge transfer is induced in the interface between the two monolayers (Figure 5). The electrons transfer from the donor layer where the surface atom has a relatively small electronegativity (Pauling electronegativity value: $F > O > H$) to the other layer (acceptor layer).[51] For this reason, the CBM level of the acceptor layer

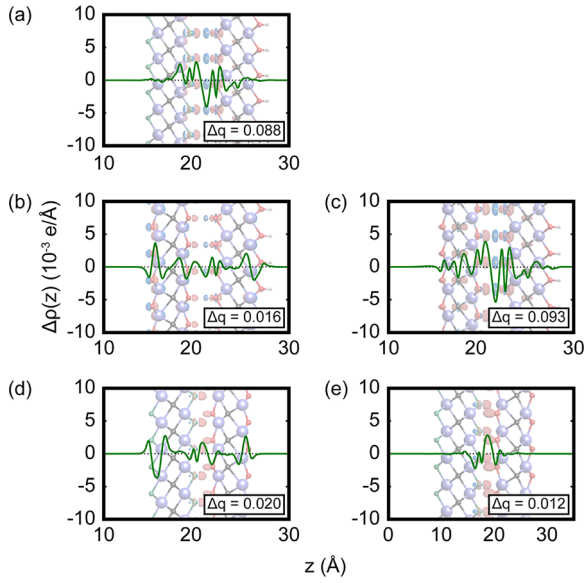

Figure 5. Charge transfer in each functionalized Sc_2C heterostructure. The plane-averaged charge density difference along the thickness direction by the heterojunction in the (a) F/OH, (b) O/OH (A), (c) O/OH (B), (d) F/O (A), and (e) F/O (B) systems. The background represents the charge redistribution, and the red and blue regions indicate the accumulation and depletion of the electrons, respectively. The isovalues are ±0.002 au. The Δq value (|e|) is the amount of the interlayer charge transfer calculated by the Bader charge.

shifts under the Fermi level (E_F) due to occupation of the electrons in the conduction band. Loss of the electrons in the valence band of the donor layer results in movement of the VBM state over the E_F (Figure 3). Thus, the charge transfer in the functionalized Sc_2C heterostructures commonly leads to a type-III heterojunction. However, although the heterojunction

DOI: 10.1021/acsami.5b00063
ACS Appl. Mater. Interfaces 2015, 7, 7163–7169

in F/O (B) also introduces the charge transfer, a band gap exists in this heterostructure as type-I.

To further understand the origin of the occurrence of the mutually different heterostructure types in the two F/O systems with the same constituents, we present the band-edge position of each monolayer relative to the vacuum level in Figure 6. Before the heterojunction, the CBM state of the

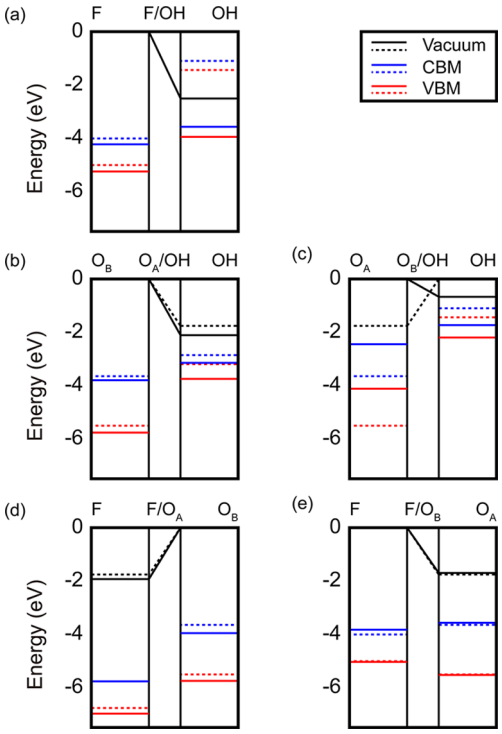

Figure 6. Band alignment of each component before and after the heterojunction: band-edge positions of the (a) F/OH, (b) O/OH (A), (c) O/OH (B), (d) F/O (A), and (e) F/O (B) systems. The dashed and solid lines represent the band alignment before and after the heterojunction, respectively. The black, blue, and red lines indicate the vacuum level at the surface of the heterosystem and the CBM and VBM levels in each monolayer, respectively. A higher vacuum level of both surfaces in each heterostructure was set to zero. The vacuum level at the other surface of the heterostructures and the CBM and VBM levels in each monolayer are presented relative to zero. Because the vacuum levels of components are the same in the interface of the heterostructure, the vacuum level in the interface was not included.

acceptor layer is located under the VBM level of the donor layer in the functionalized Sc_2C heterostructures except for the F/O (B) system. By the charge transfer during the heterojunction, the electrons with higher energy than the CBM level of the acceptor layer energetically favor transfer to the other layer to become more stable, and a broken gap occurs. On the other hand, in the F/O (B) system, the electrons of the monolayer Sc_2CO_2 cannot enter the conduction band of the acceptor layer due to their lower energy than the CBM level of the monolayer Sc_2CF_2. Instead of the transfer of the electrons to the conduction band of the acceptor layer, it was considered that the small charge transfer in the F/O (B) system can be possible by an increase in the electron density in the valence band of the Sc_2CF_2 layer. The origin that the relative CBM and VBM levels of the same two monolayers are different in the two F/O systems depending on the interface type is because each dissimilar vacuum level caused by the internal dipole moment at both surfaces of monolayer Sc_2CO_2 forms an interface with the vacuum level of the monolayer Sc_2CF_2 (Figure S5, Supporting Information). Therefore, the different vacuum levels at both surfaces by the asymmetric position of the O functional atom in the monolayer Sc_2CO_2 induce distinct heterostructure types in the two systems composed of the same monolayer Sc_2CF_2 and Sc_2CO_2.

To achieve a heterojunction type transition by the strain in these heterostructures, in type-III heterostructures, the transferred electrons should go back to the near valence band of the donor layer. However, in heterosystems including monolayer $Sc_2C(OH)_2$, the gap between the CBM and VBM levels in different layers is negligibly influenced by the strain effect (Figure S3, Supporting Information). This is because it is hard to return the electrons to the $Sc_2C(OH)_2$ layer due to the large difference in the electronegativity between the H atom of the OH functional group and the F (O) atom in the other layer.[51] Thus, only in the F/O (A) system, which has a relatively small difference in electronegativity between the two functional groups, can the heterojunction type be tuned by the strain effect among the type-III heterostructures. In the other F/O system, F/O (B), which is a type-I heterostructure, it was assumed that the heterojunction type transition is affected by alteration of a difference in work function ($\Delta\Phi$) on both surfaces in the heterostructure. The $\Delta\Phi$ is well-known to be closely related to an interface area that can be controlled by the strain.[52,53] From the change in the $\Delta\Phi$ by the strain, the levels of the vacuum, CBM, and VBM of the monolayer Sc_2CO_2 shift relative to the levels of the monolayer Sc_2CF_2, and a heterojunction type transition is possible in the F/O (B) system. Therefore, it is concluded that, by the strain, the heterojunction type can be modified in the two F/O systems among the five functionalized Sc_2C heterostructures.

CONCLUSIONS

In summary, types of heterostructures comprising three types of functionalized monolayer Sc_2C were studied using DFT calculations. In general, the type-II heterojunction is formed in the bilayer systems stacking two-dimensional semiconductors. However, special results are observed in the five functionalized Sc_2C heterostructures where the F/O (B) system becomes a type-I heterostructure, while a type-III heterojunction occurs in the other systems. It is notable that despite using the same two monolayer Sc_2CF_2 and Sc_2CO_2, distinct heterojunctions are induced in the two F/O systems by the interface including each side of the asymmetric Sc_2CO_2. In addition, the band alignment of the two F/O systems can be modulated by the strain effect and a type-II heterostructure is obtained. Interestingly, in the two type-II heterostructures, each monolayer including the CBM and VBM states is also different according to the stacking interface. Therefore, the present work establishes a novel way to create all heterojunction types with the same base material by control of the stacking interface and strain requiring only the two monolayer Sc_2CF_2 and Sc_2CO_2.

ASSOCIATED CONTENT

Supporting Information

Additional figures and information about the band structure of three monolayer components with the HSE06 functional, modeling of the functionalized Sc_2C heterostructure, change of the energy gaps in the F/OH and O/OH heterosystems by the biaxial strain, bonding character of the functionalized Sc_2C heterostructures, plane-averaged electrostatic potential of three

DOI: 10.1021/acsami.5b00063
ACS Appl. Mater. Interfaces 2015, 7, 7163−7169

monolayer components, and estimated band alignment of the F/O (B) system related to the HSE06 functional. This material is available free of charge via the Internet at http://pubs.acs.org.

AUTHOR INFORMATION

Corresponding Author

*E-mail: yongchae@hanyang.ac.kr. Tel: +82-2-2220-0507.

Notes

The authors declare no competing financial interest.

ACKNOWLEDGMENTS

This research was supported by the Basic Science Research Program through the National Research Foundation of Korea (NRF) funded by the Ministry of Education (2013R1A1A2A10064432).

REFERENCES

(1) Zhang, Q.; Zhang, Z.; Zhu, Z.; Schwingenschlogl, U.; Cui, Y. Exotic Topological Insulator States and Topological Phase Transitions in Sb_2Se_3-Bi_2Se_3 Heterostructures. *ACS Nano* **2012**, *6*, 2345−2352.

(2) Seo, H.; Posadas, A. B.; Mitra, C.; Kvit, A. V.; Ramdani, J.; Demkov, A. A. Band Alignment and Electronic Structure of the Anatase TiO_2/$SrTiO_3$ (001) Heterostructure Integrated on Si (001). *Phys. Rev. B* **2012**, *86*, 075301.

(3) Ebnonnasir, A.; Narayanan, B.; Kodambaka, S.; Ciobanu, C. V. Tunable MoS_2 Bandgap in MoS_2-Graphene Heterostructures. *Appl. Phys. Lett.* **2014**, *105*, 031603.

(4) Geng, W.; Zhao, X.; Zan, W.; Liu, H.; Yao, X. Effects of the Electric Field on the Properties of ZnO-Graphene Composites: A Density Functional Theory Study. *Phys. Chem. Chem. Phys.* **2014**, *16*, 3542−3548.

(5) Höffling, B.; Schleife, A.; Rödl, C.; Bechstedt, F. Band Discontinuities at Si-TCO Interfaces from Quasiparticle Calculations: Comparison of Two Alignment Approaches. *Phys. Rev. B* **2012**, *85*, 035305.

(6) Ramasubramaniam, A.; Naveh, D.; Towe, E. Tunable Band Gaps in Bilayer Graphene-BN Heterostructures. *Nano Lett.* **2011**, *11*, 1070−1075.

(7) Fiori, G.; Betti, A.; Bruzzone, S.; Iannaccone, G. Lateral Graphene−hBCN Heterostructures as a Platform for Fully Two-Dimensional Transistors. *ACS Nano* **2012**, *6*, 2642−2648.

(8) Kou, L.; Frauenheim, T.; Chen, C. Nanoscale Multilayer Transition-Metal Dichalcogenide Heterostructures: Band Gap Modulation by Interfacial Strain and Spontaneous Polarization. *J. Phys. Chem. Lett.* **2013**, *4*, 1730−1736.

(9) Shim, G. W.; Yoo, K.; Seo, S.-B.; Shin, J.; Jung, D. Y.; Kang, I.-S.; Ahn, C. W.; Cho, B. J.; Choi, S.-Y. Large-Area Single-Layer $MoSe_2$ and Its van der Waals Heterostructures. *ACS Nano* **2014**, *8*, 6655−6662.

(10) Zhang, H.; Zhang, Y.-N.; Liu, H.; Liu, L.-M. Novel Heterostructures by Stacking Layered Molybdenum Disulfides and Nitrides for Solar Energy Conversion. *J. Mater. Chem. A* **2014**, *2*, 15389−15395.

(11) Kośmider, K.; Fernández-Rossier, J. Electronic Properties of the MoS_2−WS_2 Heterojunction. *Phys. Rev. B* **2013**, *87*, 075451.

(12) Terrones, H.; López-Urias, F.; Terrones, M. Novel Hetero-Layered Materials with Tunable Direct Band Gaps by Sandwiching Different Metal Disulfides and Diselenides. *Sci. Rep.* **2013**, *3*, 1549.

(13) Komsa, H.-P.; Krasheninnikov, A. V. Electronic Structures and Optical Properties of Realistic Transition Metal Dichalcogenide Heterostructures from First Principles. *Phys. Rev. B* **2013**, *88*, 085318.

(14) Kou, L.; Wu, S.-C.; Felser, C.; Frauenheim, T.; Chen, C.; Yan, B. Robust 2D Topological Insulators in van der Waals Heterostructures. *ACS Nano* **2014**, *8*, 10448−10454.

(15) Geim, A.; Grigorieva, I. Van der Waals Heterostructures. *Nature* **2013**, *499*, 419−425.

(16) Naguib, M.; Kurtoglu, M.; Presser, V.; Lu, J.; Niu, J.; Heon, M.; Hultman, L.; Gogotsi, Y.; Barsoum, M. W. Two-Dimensional Nanocrystals Produced by Exfoliation of Ti_3AlC_2. *Adv. Mater.* **2011**, *23*, 4248−4253.

(17) Naguib, M.; Mashtalir, O.; Carle, J.; Presser, V.; Lu, J.; Hultman, L.; Gogotsi, Y.; Barsoum, M. W. Two-Dimensional Transition Metal Carbides. *ACS Nano* **2012**, *6*, 1322−1331.

(18) Mashtalir, O.; Naguib, M.; Dyatkin, B.; Gogotsi, Y.; Barsoum, M. W. Kinetics of Aluminum Extraction from Ti_3AlC_2 in Hydrofluoric Acid. *Mater. Chem. Phys.* **2013**, *139*, 147−152.

(19) Naguib, M.; Halim, J.; Lu, J.; Cook, K. M.; Hultman, L.; Gogotsi, Y.; Barsoum, M. W. New Two-Dimensional Niobium and Vanadium Carbides as Promising Materials for Li-Ion Batteries. *J. Am. Chem. Soc.* **2013**, *135*, 15966−15969.

(20) Peng, Q.; Guo, J.; Zhang, Q.; Xiang, J.; Liu, B.; Zhou, A.; Liu, R.; Tian, Y. Unique Lead Adsorption Behavior of Activated Hydroxyl Group in Two-Dimensional Titanium Carbide. *J. Am. Chem. Soc.* **2014**, *136*, 4113−4116.

(21) Halim, J.; Lukatskaya, M. R.; Cook, K. M.; Lu, J.; Smith, C. R.; Naslund, L.-A.; May, S. J.; Hultman, L.; Gogotsi, Y.; Eklund, P.; Barsoum, M. W. Transparent Conductive Two-Dimensional Titanium Carbide Epitaxial Thin Films. *Chem. Mater.* **2014**, *26*, 2374−2381.

(22) Gan, L.-Y.; Zhao, Y.-J.; Huang, D.; Schwingenschlögl, U. First-Principles Analysis of MoS_2/Ti_2C and MoS_2/Ti_2CY_2 (Y = F and OH) All-2D Semiconductor/Metal Contacts. *Phys. Rev. B* **2013**, *87*, 245307.

(23) Ma, Z.; Hu, Z.; Zhao, X.; Tang, Q.; Wu, D.; Zhou, Z.; Zhang, L. Tunable Band Structures of Heterostructured Bilayers with Transition-Metal Dichalcogenide and MXene Monolayer. *J. Phys. Chem. C* **2014**, *118*, 5593−5599.

(24) Er, D.; Li, J.; Naguib, M.; Gogotsi, Y.; Shenoy, V. B. Ti_3C_2 MXene as a High Capacity Electrode Material for Metal (Li, Na, K, Ca) Ion Batteries. *ACS Appl. Mater. Interfaces* **2014**, *6*, 11173−11179.

(25) Islam, M. S.; Fisher, C. A. Lithium and Sodium Battery Cathode Materials: Computational Insights into Voltage, Diffusion and Nanostructural Properties. *Chem. Soc. Rev.* **2014**, *43*, 185−204.

(26) Eames, C.; Islam, M. S. Ion Intercalation into Two-Dimensional Transition-Metal Carbides: Global Screening for New High Capacity Battery Materials. *J. Am. Chem. Soc.* **2014**, *136*, 16270−16276.

(27) Ivanovskii, A. L.; Enyashin, A. N. Graphene-like Transition-Metal Nanocarbides and Nanonitrides. *Russ. Chem. Rev.* **2013**, *82*, 735.

(28) Naguib, M.; Mochalin, V. N.; Barsoum, M. W.; Gogotsi, Y. 25th Anniversary Article: MXenes: A New Family of Two-Dimensional Materials. *Adv. Mater.* **2014**, *26*, 992−1005.

(29) Khazaei, M.; Arai, M.; Sasaki, T.; Chung, C.-Y.; Venkataramanan, N. S.; Estili, M.; Sakka, Y.; Kawazoe, Y. Novel Electronic and Magnetic Properties of Two-Dimensional Transition Metal Carbides and Nitrides. *Adv. Funct. Mater.* **2013**, *23*, 2185−2192.

(30) Khazaei, M.; Arai, M.; Sasaki, T.; Estili, M.; Sakka, Y. Two-Dimensional Molybdenum Carbides: Potential Thermoelectric Materials of the MXene Family. *Phys. Chem. Chem. Phys.* **2014**, *16*, 7841−7849.

(31) Bouhemadou, A.; Khenata, R.; Kharoubi, M.; Medkour, Y. First-Principles Study of Structural and Elastic Properties of Sc_2AC (A = Al, Ga, In, Tl). *Solid State Commun.* **2008**, *146*, 175−180.

(32) Kresse, G.; Furthmüller, J. Efficient Iterative Schemes for Ab Initio Total-Energy Calculations Using a Plane-Wave Basis Set. *Phys. Rev. B* **1996**, *54*, 11169.

(33) Kresse, G.; Furthmüller, J. Efficiency of Ab-Initio Total Energy Calculations for Metals and Semiconductors Using a Plane-Wave Basis Set. *Comput. Mater. Sci.* **1996**, *6*, 15−50.

(34) Perdew, J. P.; Burke, K.; Ernzerhof, M. Generalized Gradient Approximation Made Simple. *Phys. Rev. Lett.* **1996**, *77*, 3865.

(35) Kresse, G.; Joubert, D. From Ultrasoft Pseudopotentials to the Projector Augmented-Wave Method. *Phys. Rev. B* **1999**, *59*, 1758.

(36) Monkhorst, H. J.; Pack, J. D. Special Points for Brillouin-Zone Integrations. *Phys. Rev. B* **1976**, *13*, 5188−5192.

(37) Grimme, S. Semiempirical GGA-Type Density Functional Constructed with a Long-Range Dispersion Correction. *J. Comput. Chem.* **2006**, *27*, 1787−1799.

(38) Bucko, T.; Hafner, J.; Lebegue, Sé.; Angyán, Já. G. Improved Description of the Structure of Molecular and Layered Crystals: Ab

DOI: 10.1021/acsami.5b00063
ACS Appl. Mater. Interfaces 2015, 7, 7163−7169

Initio DFT Calculations with van der Waals Corrections. *J. Phys. Chem. A* **2010**, *114*, 11814−11824.
(39) Neugebauer, Jö.; Scheffler, M. Adsorbate-Substrate and Adsorbate-Adsorbate Interactions of Na and K Adlayers on Al (111). *Phys. Rev. B* **1992**, *46*, 16067.
(40) Heyd, J.; Scuseria, G. E.; Ernzerhof, M. Hybrid Functionals Based on a Screened Coulomb Potential. *J. Chem. Phys.* **2003**, *118*, 8207−8215.
(41) Marschall, R. Semiconductor Composites: Strategies for Enhancing Charge Carrier Separation to Improve Photocatalytic Activity. *Adv. Funct. Mater.* **2014**, *24*, 2421−2440.
(42) Shi, H.; Pan, H.; Zhang, Y.-W.; Yakobson, B. I. Quasiparticle Band Structures and Optical Properties of Strained Monolayer MoS_2 and WS_2. *Phys. Rev. B* **2013**, *87*, 155304.
(43) Zhong, X.; Yap, Y. K.; Pandey, R.; Karna, S. P. First-Principles Study of Strain-Induced Modulation of Energy Gaps of Graphene/BN and BN Bilayers. *Phys. Rev. B* **2011**, *83*, 193403.
(44) Lu, P.; Wu, X.; Guo, W.; Zeng, X. C. Strain-Dependent Electronic and Magnetic Properties of MoS_2 Monolayer, Bilayer, Nanoribbons and Nanotubes. *Phys. Chem. Chem. Phys.* **2012**, *14*, 13035−13040.
(45) Desai, S. B.; Seol, G.; Kang, J. S.; Fang, H.; Battaglia, C.; Kapadia, R.; Ager, J. W.; Guo, J.; Javey, A. Strain-Induced Indirect to Direct Bandgap Transition in Multilayer WSe_2. *Nano Lett.* **2014**, *14*, 4592−4597.
(46) Lee, Y.; Cho, S. B.; Chung, Y.-C. Tunable Indirect to Direct Band Gap Transition of Monolayer Sc_2CO_2 by the Strain Effect. *ACS Appl. Mater. Interfaces* **2014**, *6*, 14724−14728.
(47) Zhou, Y.; Li, X.; Wang, Z.; Li, S.; Zu, X. Modulating the Band Gap of Germanane Nanoribbons for Quantum Well Devices. *Phys. Chem. Chem. Phys.* **2014**, *16*, 18029−18033.
(48) Kou, L.; Li, C.; Zhang, Z.-Y.; Chen, C.; Guo, W. Charge Carrier Separation Induced by Intrinsic Surface Strain in Pristine ZnO Nanowires. *Appl. Phys. Lett.* **2010**, *97*, 053104.
(49) Björkman, T.; Gulans, A.; Krasheninnikov, A. V.; Nieminen, R. M. Van der Waals Bonding in Layered Compounds from Advanced Density-Functional First-Principles Calculations. *Phys. Rev. Lett.* **2012**, *108*, 235502.
(50) Björkman, T.; Gulans, A.; Krasheninnikov, A.; Nieminen, R. Are We van der Waals Ready? *J. Phys.: Condens. Matter* **2012**, *24*, 424218.
(51) Murphy, L. R.; Meek, T. L.; Allred, A. L.; Allen, L. C. Evaluation and Test of Pauling's Electronegativity Scale. *J. Phys. Chem. A* **2000**, *104*, 5867−5871.
(52) Anagaw, A. Y.; Wolkow, R. A.; DiLabio, G. A. Theoretical Study of Work Function Modification by Organic Molecule-Derived Linear Nanostructure on H-Silicon(100)-2 × 1. *J. Phys. Chem. C* **2008**, *112*, 3780−3784.
(53) Cho, S. B.; Yun, K.-H.; Yoo, D. S.; Ahn, K.; Chung, Y.-C. Work Function Tuning of an Ultrathin MgO Film on an Ag Substrate by Generating Oxygen Impurities at the Interface. *Thin Solid Films* **2013**, *544*, 541−544.

DOI: 10.1021/acsami.5b00063
ACS Appl. Mater. Interfaces 2015, 7, 7163−7169